Chinese Journal of Chemical Engineering 55 (2023) 181–191

Contents lists available at ScienceDirect

Chinese Journal of Chemical Engineering

journal homepage: www.elsevier.com/locate/CJChE

Full Length Article

Study on an improved rotating microchannel separator in the intensification for demulsification and separation process

Chunxin Fan [1,#], Zini Guo [2,#], Jianhong Luo [2,*]

[1] Nuclear Power Institute of China, Chengdu 610213, China
[2] Department of Chemical Engineering, Sichuan University, Chengdu 610065, China

ARTICLE INFO

Article history:
Received 23 February 2022
Received in revised form 10 May 2022
Accepted 16 May 2022
Available online 21 May 2022

Keywords:
Improved rotating microchannel (IRM)
Enhanced demulsification and separation process
Liquid–liquid two-phase flow pattern

ABSTRACT

An improved rotating microchannel (IRM) separator was further explored in the intensification for demulsification and separation process. Oil-in-water (O/W) emulsion system of 2-ethylhexyl phosphoric acid-2-ethylhexyl ester (P507)–water without emulsifier was employed to evaluate the performance of the new equipment. In this experiment, the influence on demulsification separation process was explored by changing the geometrical structure and channel height of the microchannel and combining the liquid–liquid two-phase flow pattern, and the correlation general graph between demulsification efficiency and dimensionless parameters was established. The total demulsification effect of the IRM and the separation capacity of the clear organic phase recovered from demulsification are significantly improved. In addition, the liquid–liquid two-phase flow pattern of the clear organic phase after demulsification and the remaining emulsion in the IRM are observed and recorded by high-speed photography. The separation ability of organic phase from the upper outlet can be significantly improved when the total demulsification rate of IRM is up to 90%. There are 3 types and 6 kinds of flow patterns observed. The results demonstrated that the suitable demulsification performance is obtained when the liquid–liquid two-phase inside the IRM is in a parallel pattern. Finally, the relation map between total demulsification efficiency and the universal flow is drawn, which provides a basis for the accurate control of the IRM device.

1. Introduction

With the continuous development of economy and society, oil products are widely used in human daily life. Although oil products bring people a lot of convenience, they also bring pollution [1–3]. According to the environmental protection law, oily sewage and oil–water mixture must be recycled and treated up to standard before being discharged [4]. Therefore, it is significant and necessary to effectively recover and remove dispersed organic phase from the continuous aqueous phase.

In recent years, microchannels have attracted more and more attention because of their small size, high mass transfer efficiency and numerical amplification [5,6]. The microchannels reported in the existing literature mainly include T-junction, Y-junction, *etc.* [7–10]. Researchers specifically studied the structure, internal mass transfer, flow pattern and optimization of process parameters of such microchannels [11–13]. These microchannels are based on passive mixing microchannels, that is, the internal fluid flow changes by changing the structure of the microchannels. However, there are few microchannels with active mixing in the published literature.

Therefore, this research group designed a rotating microchannels (RM) based on the idea of microchannels, hydrophilic, hydrophobic materials and centrifugation. Although the RM has good demulsification performance, the demulsified organic phase cannot be separated well from the upper outlet well [14]. The effect of demulsification and phase separation was further enhanced by changing the geometry of the improved rotating microchannel (IRM) in this experiment, which has great influence on demulsification effect. In addition, the liquid–liquid two-phase flow pattern formed in the IRM has a significant impact on the demulsification and separation of the oil-in-water (O/W) emulsion system. The mixing process of microchannel demulsification is worthy of systematic study [15–18]. Therefore, the flow state of organic phase and residual emulsion in the IRM can be intuitively observed in this experiment.

The 2-ethylhexyl phosphoric acid-2-ethylhexyl ester (P507) is used as a common extractant to remove metal cations [19,20]. Emulsification extraction with the P507 extractant is a very effective separation method [21]. The demulsification effect of

* Corresponding author. Fax: +028 62137696.
E-mail address: luojianhong@scu.edu.cn (J. Luo).
# These authors contributed equally to this work.

https://doi.org/10.1016/j.cjche.2022.05.002
1004-9541/

P507-water emulsion in the IRM without surfactant was studied. The influence of the microchannel height (H) and the microchannel geometry diameter (d_1) on demulsification and separation process was studied, and universal flow map between demulsification efficiency and dimensionless parameters was established.

2. Experimental

2.1. Materials

Kerosene and P507 as organic phases were produced by Luoyang Zhongda Chemical Co., Ltd., China (AR grade). The emulsifier, sodium dodecyl sulfate (SDS), was purchased from Chengdu Jinshan Chemical Co., Ltd., China (AR grade). The physical properties of the dispersed phases are listed in Table 1. Solutions were prepared using deionized water. All chemicals were used without further purification.

2.2. Experimental setup

Fig. 1 shows the schematic diagram of the IRM device, the inner cylinder is made of lipophilic polytetrafluoroethylene (PTFE), and the outer cylinder is made of hydrophilic plexiglass (PMMA), so as to facilitate the observation of the internal flow. At the same time, because of the different hydrophilic material of the inner and outer cylinder, emulsification of oil and water phase can be avoided.

The experimental process is shown in Fig. 2, which mainly includes microchannel demulsification system, fluid transport control system and image acquisition system. The emulsion was transported by an advection pump. The feed flow rate of oil–water phase varied from 1 to 8 ml·min^{-1} and the feed ratio was controlled at 1:1. Demulsification and phase separation were carried out after the emulsion entered the rotary scraping microchannel. Finally, the clear organic phase and the remaining emulsion that was not completely demulsified were collected at the upper and lower discharge ports. The high-speed camera is used to observe and record the flow of two-phase fluid in the microchannel in real time, and the images or dynamic images are saved in the memory of the computer.

2.3. Measurement of demulsification efficiency

The demulsification efficiency of the upper outlet of the IRM is based on the amount of clarified organic phase flowing out of the PTFE outlet of the IRM. Demulsification efficiency (E_{up}) at the upper outlet is defined by the following:

$$E_{up} = \frac{V_{clear,o,up}}{V_{initial,total} \times \varphi_o} \quad (1)$$

where, the $V_{initial,total}$, $V_{clear,o,up}$ and φ_o represent the initial volume of the emulsion, the volume of the clarified organic phase from the PTFE outlet and the organic phase content of the initial emulsion. E_{up} represents the ability of the upper outlet to recover the organic phase from the O/W emulsion.

The demulsification efficiency of the lower outlet of the microchannel is based on the amount of clarified organic phase flowing from the PMMA outlet of the IRM. Demulsification efficiency (E_{low}) at the lower outlet is defined by the following:

$$E_{low} = \frac{V_{clear,o,low}}{V_{initial,total} \times \varphi_o} \quad (2)$$

where $V_{clear,o,low}$ represents the volume of the clear organic phase from the PMMA outlet. E_{low} represents the ability of the IRM lower outlet to recover the clarified organic phase from oil-in-water (O/W) emulsion.

Table 1
Physical properties of the working systems at 25 °C

Working system	Density, ρ/kg·m^{-3}	Viscosity/mPa·s	Interfacial tension, σ_{o-a}/μg·m^{-3}
Water	997.0	0.8937	/
20% P507	789.3	2.4963	/
40% P507–water emulsion	915.8	3.2980	20.47

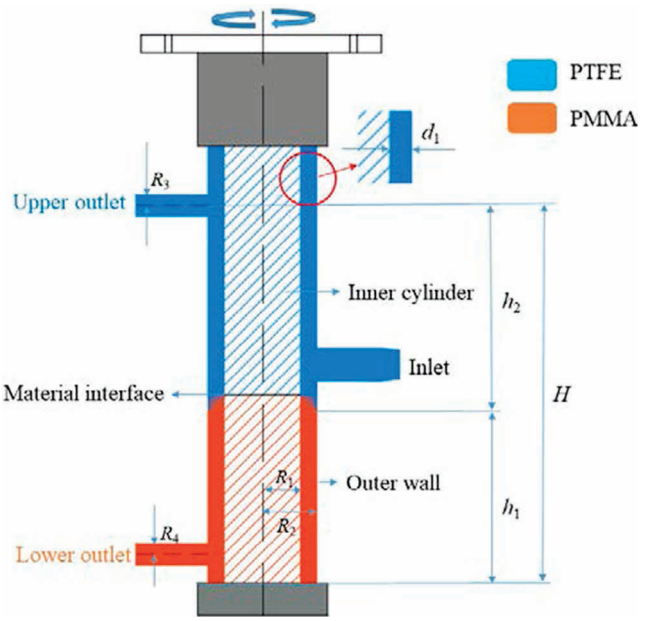

Fig. 1. Schematic diagram of the IRM device.

The total demulsification efficiency (E_{total}) is defined by the following formula:

$$E_{total} = \frac{V_{clear,o,low} + V_{clear,o,up}}{V_{initial,total} \times \varphi_o} \quad (3)$$

where E_{total} represents the capacity of the IRM to demulsify and recover the clear organic phase from O/W emulsion. Our research group hopes that the demulsified and recovered clear organic phase will flow out from the upper outlet as far as possible, and the remaining emulsion will flow out from the lower outlet, namely, higher E_{total} and E_{up}, and lower E_{low} as far as possible.

E_{total} is the total capacity of the IRM to recover the clarified organic phase from O/W emulsion. In our experiment, operation is stable. All of our experimental results are consistently stable as follows:

$$\frac{(V_{clear,o,up} + V_{remain,up}) + (V_{clear,o,low} + V_{remain,low})}{V_{initial,total}} > 96\% \quad (4)$$

where $V_{remain,up}$ and $V_{remain,low}$ represent the volume of the remaining emulsion that has not been demulsified from the upper and lower exits of the IRM respectively. According to the expression of Eq. (4), our experimental operation is stable.

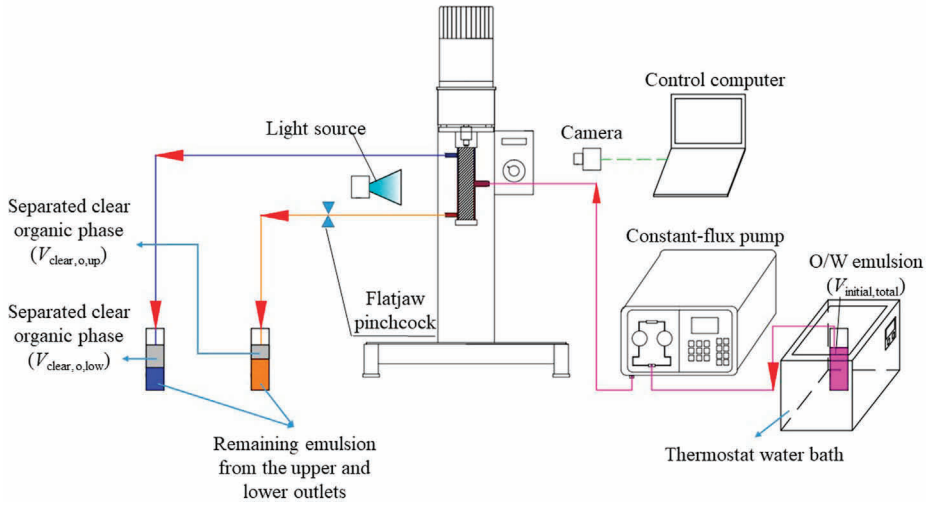

Fig. 2. Schematic diagram of experimental devices for the study of different microchannel geometry and related flow patterns.

3. Results and Discussion

3.1. Effect of microchannel height (residence time)

Fig. 3 shows the influence of different microchannel heights on the total demulsification rate of the IRM, and the values of microchannel height are listed in the Supplementary Material. The effects of residence time and centrifugal inertia force on the demulsification effect of the IRM are competitive [22–24]. When the inner cylinder speed (R) is lower than 300 r·min^{-1}, the total demulsification rate increases with the increase of microchannel height. This is because with the increase of height, the fluid flow space inside the IRM becomes larger, resulting in the residence time of emulsion in the IRM. It indicates that the demulsification effect of the IRM is mainly dominated by residence time when the R is lower than 300 r·min^{-1} and the centrifugal inertia force is low. When the R is higher than 300 r·min^{-1}, the demulsification results are almost the same at different microchannel heights. It indicates that the demulsification effect of the IRM is mainly dominated by centrifugal inertia force when the centrifugal inertia force is high.

Fig. 4 respectively shows the demulsification efficiency comparison of the upper outlet and the lower outlet with different microchannel heights.

When the height of the microchannel increases, the residence time increases, and the demulsification rate at the outlet of the three types of microchannel heights all increase significantly. On the one hand, as the height of the microchannel increases, the u_z remains unchanged, so the increase of residence time is conducive to the enhancement of demulsification effect. On the other hand, since the geometric diameter of the IRM is only 0.15 mm, the narrow space promotes the clear organic phase and the remaining emulsion to form a parallel flow (PF) when the rotation speed is more than 300 r·min^{-1}. Therefore, the clear organic phase produced by demulsification cannot migrate to the upper outlet due to the PF. Instead, the ring-shaped clear organic phase is pushed by the ring-formed residual emulsion to the lower outlet.

When the microchannel height increased, the demulsification rate at the upper outlet of the IRM with the height of 9 and 15 cm increased significantly at first and then decreased slightly at the rotation speed of 100 –500 r·min^{-1}. However, the IRM with a height of 19 cm was significantly increased first and then slightly increased. This shows that under the action of higher centrifugal inertial force, when the residence time increases to a certain threshold, the demulsification rate of the upper outlet is mainly affected by the centrifugal inertial force. In addition, as shown in Fig. 4, the outflow of lighter organic phase from the upper outlet is not good. The E_{up} is higher than E_{low} only appeared at the height of 9 and 15 cm, and the speed range was the largest at the height of 9 cm. However, when the height is 19 cm, E_{up} is lower than E_{low} at 100 –500 r·min^{-1}. There are two main reasons for this situation: First, with the increase of microchannel height, although the residence time of the emulsion increases, u_z remains unchanged, and the larger space of the IRM takes longer time for the lighter organic phase to migrate to the upper outlet; second, due to the high centrifugal inertia force, the PF formed inside the IRM limits the normal migration of organic phase, making it difficult to obtain a high E_{up}.

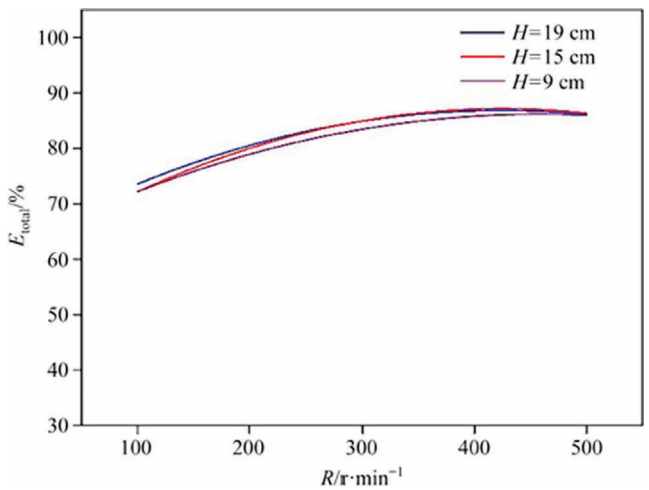

Fig. 3. The effects of microchannel height on the total demulsification efficiency. Conditions: system = P507–water emulsion; d_1 = 0.15 mm; $Q_{em,in}$=1 ml·min^{-1}; T_{in} = 25 °C; T = room temperature (~25 °C).

In summary, the residence time is the dominant factor at low speeds for the E_{total} of the IRM. At high rotation speed, centrifugal inertia force is the main control factor. For the E_{up} and E_{low} of the IRM, that is, the separation effect of the upper outlet, the residence time is the dominant factor at low speeds. At high speeds, both residence time and centrifugal inertia are important influencing factors.

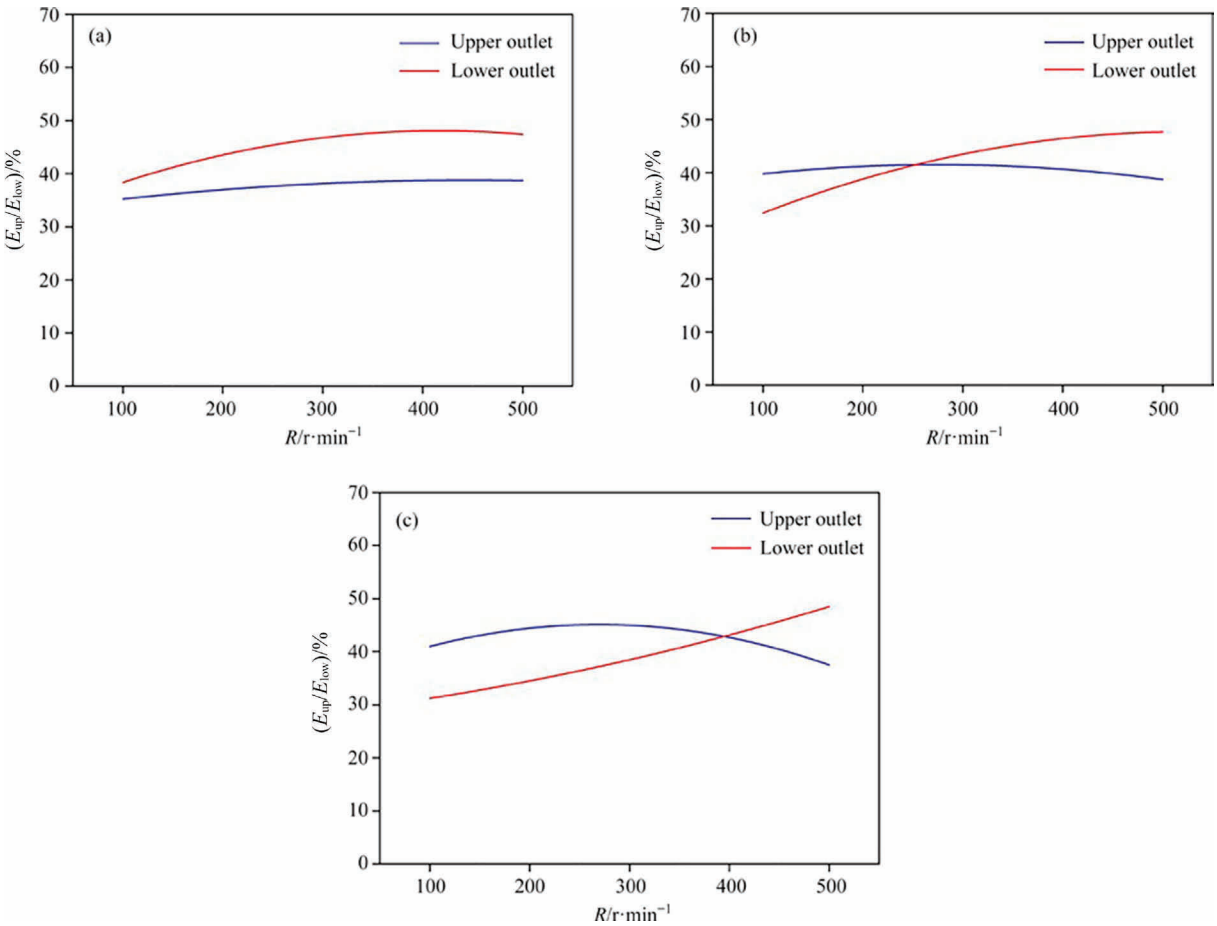

Fig. 4. The effects of microchannel height on the demulsification efficiency of the upper and lower outlets: (a) H = 19 cm; (b) H = 15 cm; (c) H = 9 cm. Conditions: system = P507–water emulsion; d_1 = 0.15 mm; $Q_{em,in}$ = 1 ml·min^{-1}; T_{in} = 25 °C; T = room temperature (~25 °C).

3.2. Effect of microchannel geometry diameter

In order to explore the influence of microchannel geometric diameter (d_1) on the demulsification and separation effect of the IRM, three different d_1 of 0.15, 0.35 and 0.55 mm were used in the experiment. Fig. 5(a) shows that at the full speed of 0–700 r·min^{-1}, the total demulsification rate of the IRM decreases to a certain extent as d_1 increases. Fig. 5(b) shows that the $V_{remain,total}$ increases to a certain extent with the increase of d_1. This shows that the reduction of the d_1 is beneficial to the enhancement of the demulsification effect of the IRM.

Since the height of the IRM (19 cm) is much larger than that of d_1 (0.15–0.55 mm), the effective demulsification and separation surfaces of the IRM are the inner drum and the outer wall (Table 2).

The detailed calculation formulas are listed in the Supplementary Material. Where V and S are the volume and surface area of effective demulsification and separation of the IRM, H is the geometric height of the IRM, R_1 and R_2 are the inner drum and outer wall radius of the microchannel, d_1 is the geometric diameter of the microchannel, D is the particle diameter of emulsion droplets, and r is the particle radius of emulsion droplets.

The influence of restriction ratio on E_{total} is shown in Fig. 6. As the restriction ratio increases, the total demulsification rate of the IRM is higher. In addition, it can be concluded that when the centrifugal inertia force is lower, the total demulsification rate of the IRM with the higher the restriction ratio increases more obviously. At this time, the demulsification effect is mainly dominated by the restriction effect of the IRM on the emulsion. When the centrifugal inertia force is higher, the increase of the total demulsification rate of the IRM with the higher the restriction ratio slows down. At this time, the demulsification effect is mainly dominated by the centrifugal inertia force.

This shows that even when the droplet size (particle size < 10 μm) is much smaller than the d_1 (150–550 mm), the restriction effect of the microchannel on the emulsion droplets cannot be completely ignored. When the restriction ratio reaches a certain threshold, combined with the centrifugal inertial force, the flow of the emulsion in the IRM presents new characteristics. As shown in Fig. 7, the organic phase demulsified by the three different d_1 at higher speeds has a restricted PF.

Although the IRM has good demulsification effect, the separation effect of clear organic phase produced by self-demulsification is not very good. The higher E_{up} of the IRM, the better the separation effect of the IRM. When the rotation speed of the inner cylinder is too high, the clear organic phase from demulsification is not easy to flow out of the upper outlet. Fig. 8 shows the comparison of the demulsification efficiency of different d_1 for the upper outlet and the lower outlet. The figure shows that when d_1 is increased, the E_{up} is significantly higher than the E_{low}. When d_1 = 0.15 mm, the E_{up} and E_{low} are almost the same; while d_1 = 0.55 mm, the E_{up} is much higher than the E_{low} (>40%). This is due to the weakening of the limiting effect by increasing d_1. As shown in Fig. 8, the larger d_1 is, the more difficult it is for the clear organic phase and the remaining emulsion to form PF at high speed

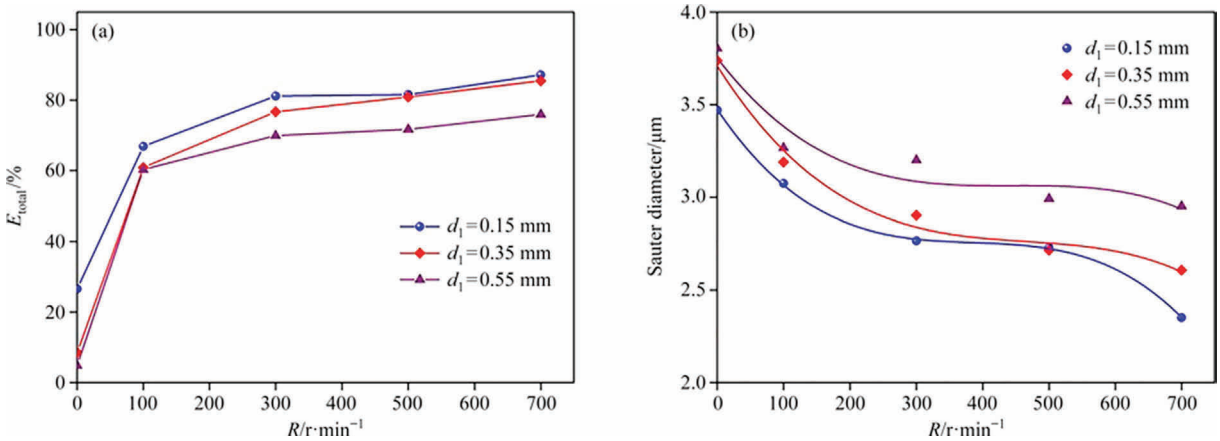

Fig. 5. Demulsification results of different microchannel diameters. Effects of microchannel geometric diameter on the (a) total demulsification efficiency; (b) Sauter diameter of the remaining emulsion from the upper and lower confluence after the IRM demulsification. Conditions: system = P507–water emulsion; H = 19 cm; $Q_{em,in}$=2 ml·min^{-1}; T_{in} = 25 °C; T = room temperature (~25 °C).

Table 2
The restriction ratio of different microchannel geometric diameters

d_1/μm	R_2/m	R_1/m	H/m	S/m^2	V/m^3	D/d_1
150	0.0098	0.00965	0.19	0.023208	1.7406×10^{-6}	0.0275333
350	0.0098	0.00945	0.19	0.022969	4.0196×10^{-6}	0.0118000
550	0.0098	0.00925	0.19	0.022730	6.2509×10^{-6}	0.0075091

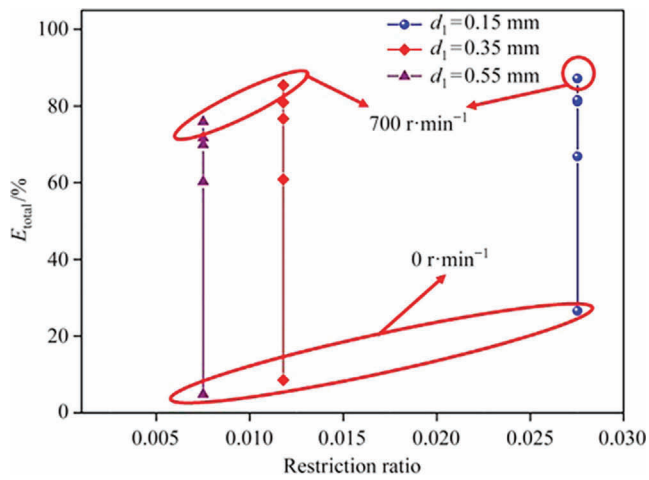

Fig. 6. The effect of the restriction ratio on the total demulsification efficiency. Conditions: system = P507–water emulsion; H = 19 cm; $Q_{em,in}$=2 ml·min^{-1}; T_{in} = 25 °C; T = room temperature (~25 °C).

(500 r·min^{-1}). Therefore, the demulsified organic phase is pushed by the remaining emulsion to the lower outlet of the IRM due to the formation of PF.

In summary, when the droplet size (<10 μm) is much smaller than the d_1 (150–550 mm), the restriction effect of the IRM causes the emulsion droplets to collide with each other more frequently and hit the wall. This further leads to instability and coalescence of the emulsion droplets. On the one hand, the IRM with a higher restriction ratio (restriction ratio = 0.0275333, d_1 = 0.15 mm) has a very attractive E_{total}. On the other hand, appropriately lowering the restriction ratio (0.0075091, d_1 = 0.55 mm) of the IRM will sacrifice a small part of the E_{total}, but it will greatly improve the E_{up}.

3.3. The relation map of E_{total}

The IRM is a kind of microchannel equipment with externally induced forced disturbance. Its operating parameters are $Q_{em,in}$ and R, and structural parameters of H and d_1 both have a certain influence on the demulsification effect of the emulsion. In order to better control the IRM and make it work in the region of high demulsification efficiency, it is necessary to more accurately control the operating parameters in the rotating wiped film microchannel reactor. It is difficult to determine the optimal operating conditions directly in an operation diagram under the combined action of all the operating parameters mentioned above. To solve this problem, the research group referred to the processing method of Zhao *et al.* [25]. The above operating parameters were included in the influence of fluid inertial force and surface tension, and the *We* number was used to correlate with the E_{total}.

Since the d_1 is only 150–550 μm, the fluid in the IRM mainly exhibits two-dimensional motion in the vertical and tangential directions. This study ignores the radial velocity of the fluid in the IRM.

The fluid velocity (u_z) in the vertical direction is defined as follows:

$$u_z = \frac{Q_{em,in}}{\pi(R_2^2 - R_1^2)} \tag{5}$$

In this study, there are the following assumptions:

(1) Assume that the vertical velocity of the organic phase is the same as the vertical velocity of the water phase, that is $u_{z,o} = u_{z,a}$.
(2) Assume that the tangential velocity of the organic phase and the tangential velocity of the water phase have the same distribution, that is $u_{\theta,o} = u_{\theta,a}$.

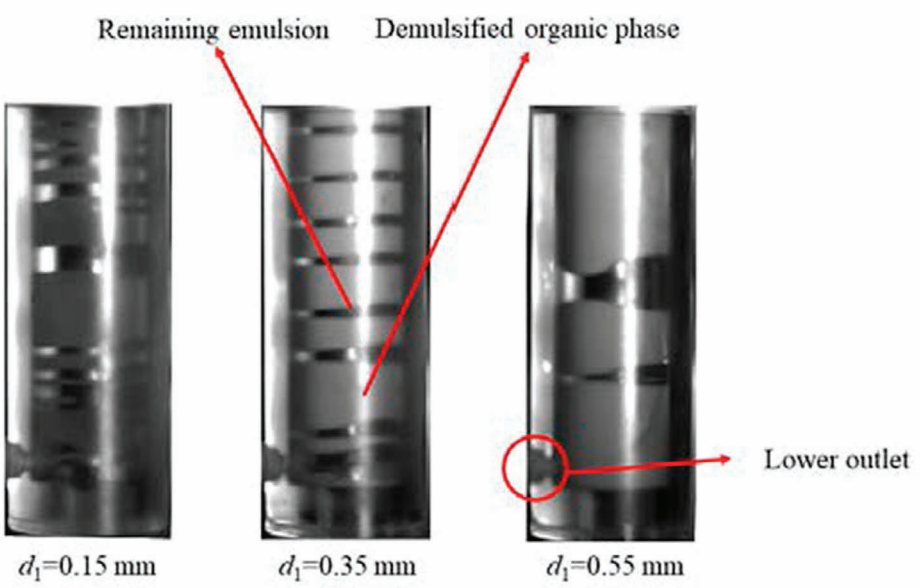

Fig. 7. Liquid–liquid two-phase flow patterns with different feed volume flow rates. Conditions: system = P507–water emulsion; H = 19 cm; $Q_{em,in}$=2 ml·min^{-1}; R = 500 r·min^{-1}; T_{in} = 25 °C; T = room temperature (~25 °C).

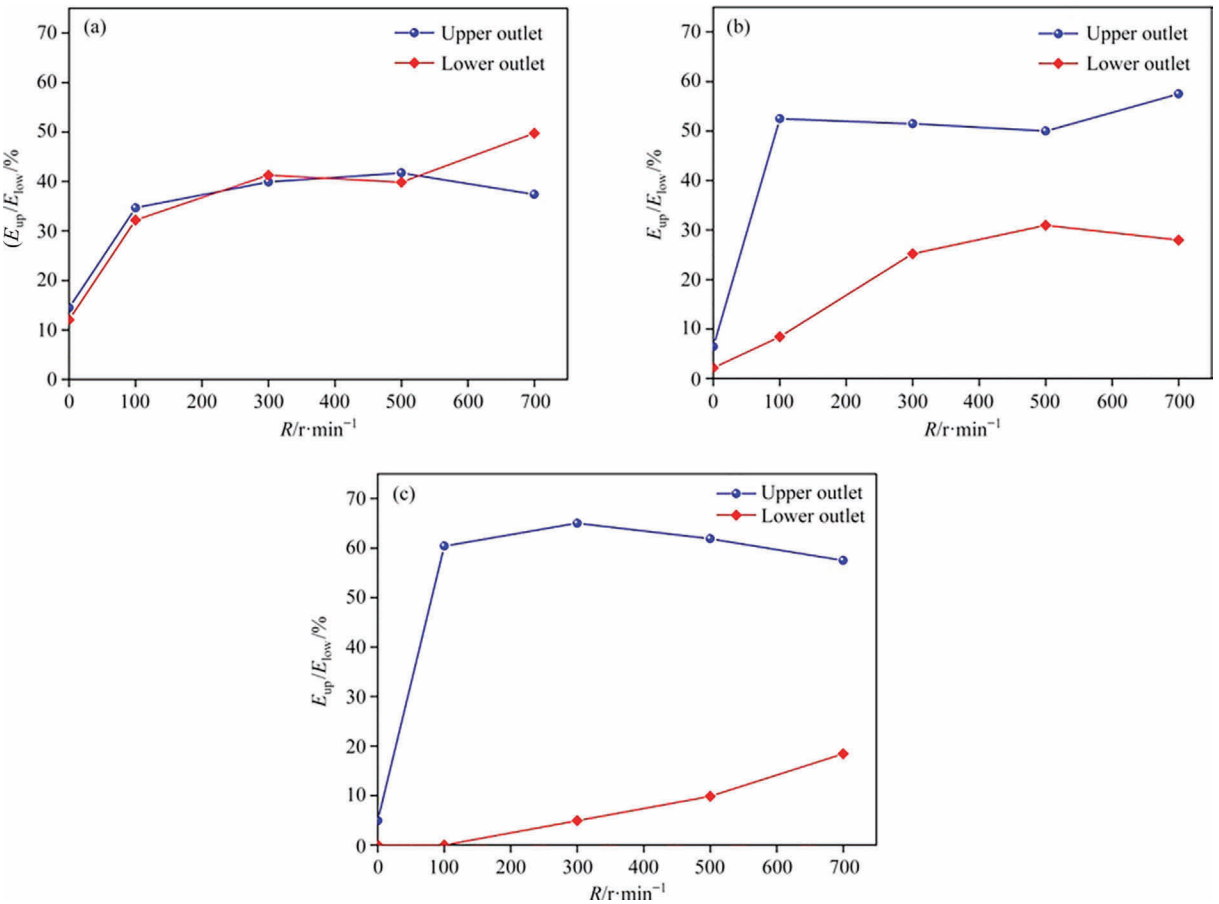

Fig. 8. The effects of microchannel geometric diameter on the demulsification efficiency of the upper and lower outlets: (a) d_1 = 0.15 mm; (b) d_1 = 0.35 mm; (c) d_1 = 0.55 mm; Conditions: system = P507–water emulsion; H = 19 cm;$Q_{em,in}$ = 2 ml·min^{-1}; T_{in} = 25 °C; T = room temperature (~25 °C).

The average tangential velocity is expressed as:

$$\bar{u}_\theta = \frac{2\pi k^2 R}{60(1-k^2)}\left(R_2^2 \ln\frac{R_2}{R_1} - \frac{R_2^2 - R_1^2}{2}\right) \times \frac{1}{R_2 - R_1} \quad (6)$$

The detailed calculation formulas are listed in the Supplementary Material.

The experimental system in this chapter is a P507–water O/W emulsion without emulsifier. The aqueous phase is the continuous phase and the organic phase is the dispersed phase in the form of small droplets. The IRM is used to recover the organic phase in the oil-in-water emulsion as much as possible, based on the above assumption that u_z and u_θ of the organic phase and the water phase are the same. Therefore, the *We* number of dispersed organic phases is mainly concerned in calculation and processing. The specific calculation steps are as follows:

The *We* number in the vertical direction of the organic phase ($We_{z,o}$):

$$We_{z,o} = \frac{\rho_o u_{z,o}^2 d_1}{\sigma_{o-a}} \quad (7)$$

The *We* number in the tangential direction of the organic phase ($We_{\theta,o}$):

$$We_{\theta,o} = \frac{\rho_o u_{\theta,o}^2 d_1}{\sigma_{o-a}} \quad (8)$$

The correlation of $We_{z,o}$, $We_{\theta,o}$ and E_{total} in the operating parameters in this chapter is shown in Fig. 9, it can be seen from the figure that $We_{z,o}$ is controlled below 0.0001, and $We_{\theta,o}$ is controlled between 0.15–0.5. Alternatively, $We_{z,o}$ can be controlled at 0.0001–0.0004, and $We_{\theta,o}$ can be controlled at more than 0.5, so that the IRM can work in the area of high demulsification efficiency.

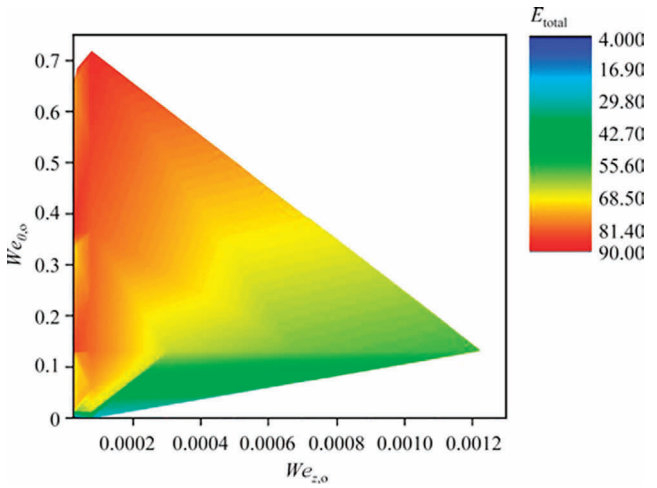

Fig. 9. Relation map of $We_{z,o}$–$We_{\theta,o}$–E_{total}. Conditions: system = P507–water emulsion; H = 9–19 cm; d_1 = 0.15–0.55 mm; R = 0–700 r·min^{-1}; $Q_{em,in}$=1–8 ml·min^{-1}; T_{in} = 25 °C; T = room temperature (~25 °C).

3.4. Study on liquid–liquid two-phase flow pattern in the IRM

3.4.1. Types of liquid–liquid two-phase flow patterns in microchannels

The liquid–liquid two-phase flow patterns of the demulsified clear organic phase (organic phase) and the remaining emulsion that was not demulsified (emulsion phase) in the lower half of the IRM were observed and recorded.

Fig. 10 shows experimentally observed flow patterns of two-phase flow in the IRM at different speeds, flow rates and different channel sizes. According to the distribution of organic phase and emulsion phase produced by demulsification and the different shapes of organic phase droplets, the flow patterns inside the IRM are roughly divided into 6 types. They are the organic phase droplet-emulsion continuous flow (D-CF, Fig. 10(a)), the long organic phase droplets-emulsion phase continuous flow (LD-CF, Fig. 10(b)), and the organic phase annular-emulsion band flow (P-BF, Fig. 10(c)), organic phase band-emulsion band flow (B-BF, Fig. 10(d)), organic phase continuous-emulsion continuous flow (C-CF, Fig. 10(e)) and full emulsion continuous flow (FCF, Fig. 10(f)).

C-CF (d_1 = 0.15 mm) is that when the inner drum is stationary, the distribution of organic phase and emulsion phase mainly comes from the wetting action of the inner drum and the outer wall. The stronger the restriction ratio or the larger the specific surface area of the IRM, the greater the influence of interfacial tension [26]. When D-CF and L-CF are at a low centrifugal inertia, the organic phase is slightly deformed by the action of the inner drum. At the same time, the organic phase cannot rise to the upper outlet in time due to the large limiting effect (d_1 = 0.15 mm) and can only be carried to the lower outlet by the emulsion phase. P-BF and B-BF are mainly caused by strong centrifugal inertia force. FCF is mainly due to the weakening of the internal limiting effect of the IRM (d_1 = 0.35–0.55 mm). Due to the density difference, most of the organic phase can migrate to the upper outlet, while the emulsion phase can migrate to the lower outlet. The above shows that the liquid–liquid two-phase fluid in the IRM is mainly affected by gravity, centrifugal force and surface tension [27,28], thus showing different flow patterns.

3.4.2. Factors of liquid–liquid two-phase flow pattern change

In this study, the main factors affecting the liquid–liquid two-phase flow patterns of organic phase and emulsion phase are $Q_{em,in}$, R and d_1. Fig. 11 reflects the influence of the above factors on the flow patterns in the IRM, and the six flow patterns are roughly divided into three categories.

The first type is continuous flow pattern, which includes C-CF and FCF, mainly because of the IRM with low rotational speed. FCF mainly occurs in the IRM with d_1 of 0.35 and 0.55 mm. Due to the large d_1 of the IRM in this case, the centrifugal inertia force and the internal restriction effect of the IRM are weak. Due to the effect of gravity, the lighter organic phase is easier to migrate to the upper outlet, while the heavier residual emulsion phase is deposited to the lower half to form FCF. When d_1 is as small as 0.15 mm, the restriction effect of the IRM is enhanced, the organic phase that has no time to migrate upwards and the remaining emulsion phase form C-CF in the lower half. The first type of flow pattern is mainly influenced by gravity.

When the rotation speed and the feed flow rate increase, the first type of flow pattern gradually forms the second type of droplet flow pattern. The second type includes D-CF and LD-CF. The main reason for the formation of D-CF and LD-CF is that the centrifugal inertial force and vertical macroscopic flow rate have increased to a certain extent. The clear organic phase from demulsification cannot be removed from the upper outlet in time due to the non-negligible restriction effect of the IRM and large u_z. The second type of droplet flow pattern is mainly dominated by R, $Q_{em,in}$ and d_1.

When the speed continues to increase, the second major type of flow patterns (D-CF and LD-CF) gradually form the third type, that is, parallel flow patterns, and the third type includes P-BF and B-BF. With strong centrifugal inertia force and internal restriction of the IRM (d_1 = 0.15–0.35 mm), the demulsified organic phase forms a thin ring, while the remaining emulsion phase is divided into annular band. Because the narrow space inside the IRM cannot migrate to the upper outlet, the annular organic phase is pushed

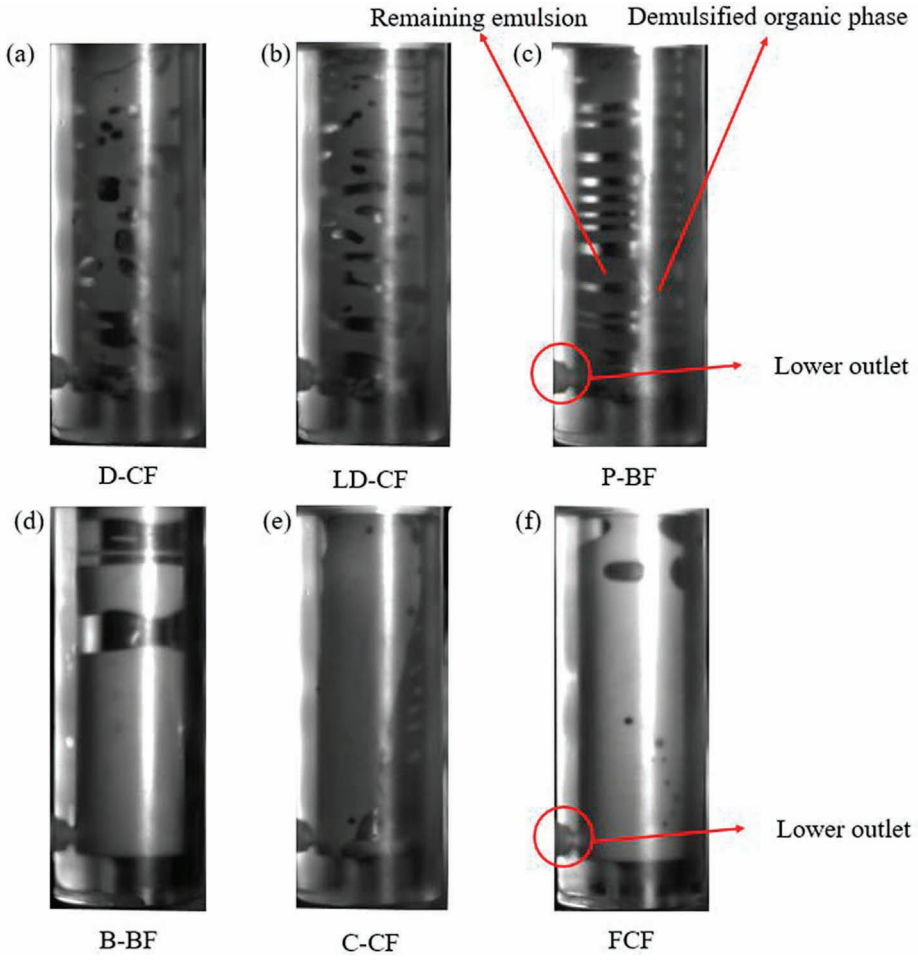

Fig. 10. Flow patterns in the IRM: (a) D-CF; (b) LD-CF; (c) P-BF; (d) B-BF; (e) C-CF; (f) FCF.

to the lower outlet, so the P-BF is formed. When the restriction effect of the IRM is weakened (d_1 = 0.35–0.55 mm), the organic phase is easier to migrate upward and more difficult to form a thin ring. As the centrifugal force continues to increase, more organic phases are demulsified and a more stable and coarser annular band flow is formed. Similarly, the stable annular organic phase is not easy to disperse into droplets and migrate upward, but is pushed to the lower outlet by the banded emulsion phase to form B-BF. According to the above discussion, the third type flow pattern is mainly dominated by R and d_1.

Zhao *et al.* [25] used the *We* number to divide the flow pattern at the liquid–liquid joint in the T-type equipment into three regions (region I, region II, and region III).

This study calculates the *We* number of the organic phase and the emulsion phase. The water phase is the continuous phase, and the organic phase is the dispersed phase in the form of small droplets. Therefore, the *We* numbers of the emulsion in this work were calculated and compared with the experimental results of Zhao *et al.*, the *We* number of the organic phase and the remaining emulsion without demulsification are calculated as follows:

$$We_o = \frac{\rho_o u_o^2 d_1}{\sigma_{o-a}}$$
$$We_a = \frac{\rho_a u_a^2 d_1}{\sigma_{o-a}} \quad (9)$$

The comprehensive velocity u_o and u_a of emulsion phase are shown in Eq. (10):

$$u_o = \sqrt{\bar{u}_{\theta,o}^2 + u_{z,o}^2}$$
$$u_a = \sqrt{\bar{u}_{\theta,a}^2 + u_{z,a}^2} \quad (10)$$

The calculated *We* numbers ($1.4 \times 10^{-6} < We_o < 5.9 \times 10^{-2}$, $1.8 \times 10^{-6} < We_a < 7.5 \times 10^{-2}$, 100 r·min^{-1} < R < 200 r·min^{-1}) of the P507 − water emulsion contain the zone I, where the interfacial tension dominated. The flow patterns of the emulsion and organic phases (D-CF, LD-CF, P-BF, C-CF, FCF) correspond to the flow patterns of the monodispersed droplet (MDT) presented by Zhao *et al.* The calculated *We* numbers ($1.1 \times 10^{-1} < We_o < 7.2 \times 10^{-1}$, $1.5 \times 10^{-2} < We_a < 9.0 \times 10^{-1}$, 300 r·min^{-1} < R < 700 r·min^{-1}) of the P507 − water emulsion still contains region I. With the increase of the inner cylinder speed, the centrifugal inertia force increases, and the inertia force and interfacial tension affect the flow pattern together. The flow patterns of emulsion and organic phases mainly correspond to the parallel flow (PFST) of Zhao *et al.* [25]. Therefore, there was an agreement between the results of our work and those of others [29,30].

3.4.3. Universal flow map

In the early literature, Buckingham *et al.* [31] proposed a dimensionless analysis. Therefore, the flow pattern can be specified by various dimensionless numbers. The value of the flow pattern map is to predict the flow pattern that is conducive to demulsification and separation. Zhao *et al.* [25] and Cherlo *et al.* [32] suggested using the *We* number to display the flow pattern. In this flow pattern, the influence of various parameters (such as physical, struc-

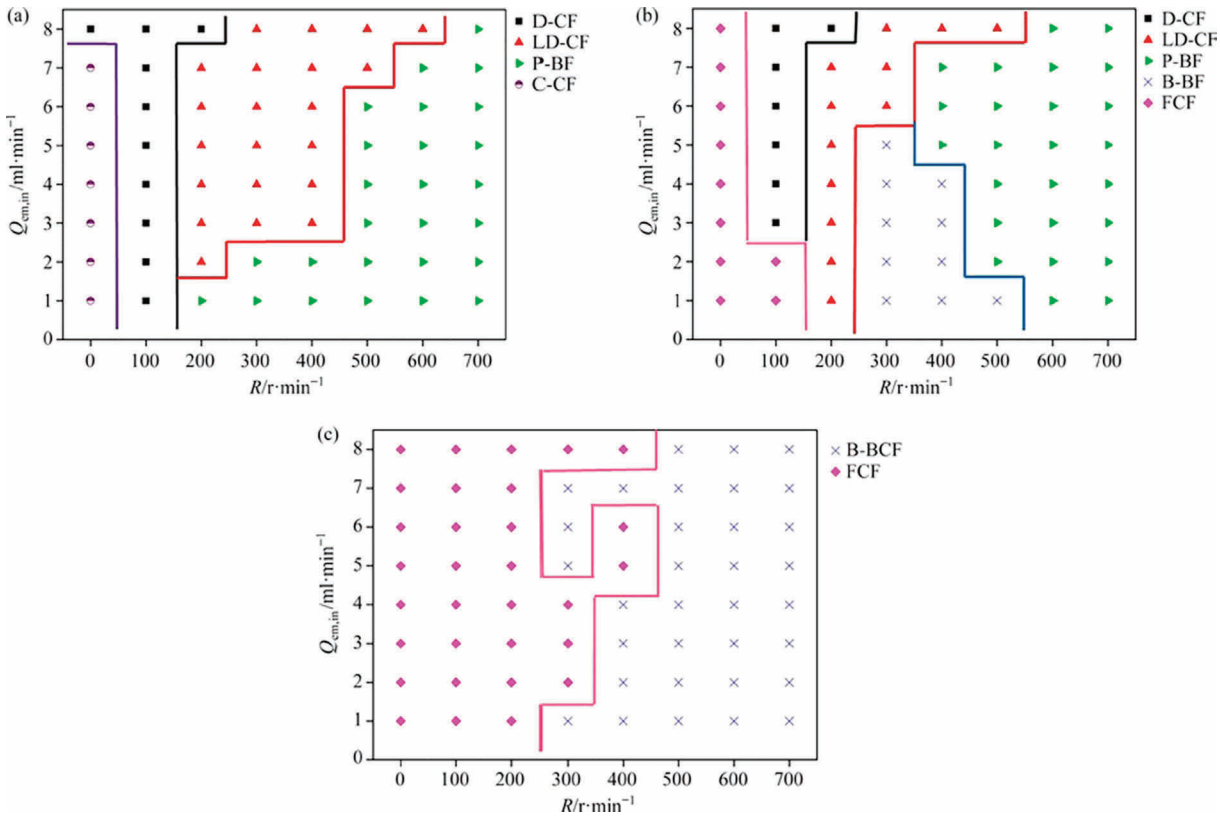

Fig. 11. Flow pattern in the IRM under different equipment and operation parameters: (a) d_1 = 0.15 mm; (b) d_1 = 0.35 mm; (c) d_1 = 0.55 mm; Conditions: system = P507–water emulsion; H = 19 cm; T_{in} = 25 °C; T = room temperature (~25 °C).

tural and operational parameters) on the flow pattern should be considered. The Oh number ($Oh = \mu/(\rho\sigma d_1)^{1/2}$) is a dimensionless number, which represents the ratio of viscous force to inertia and surface tension. Yagodnitsyna *et al.* [33] and Darekar *et al.* [34] use "$We{\cdot}Oh$" as a new parameter, which includes various parameters (ρ, μ, σ, d_1, u). They are in good agreement with the data presented by Zhao *et al.* [25] and Kashid *et al.* [30]. Therefore, this experiment with oil-in-water emulsion demulsification of target and the recycling of dispersed organic phase as the object, select "$We_{\theta,o} \cdot Oh_o$" and"$We_{\theta,o} \cdot Oh_o$" to represent the demulsification out clear organic phase respectively in the IRM of the effect

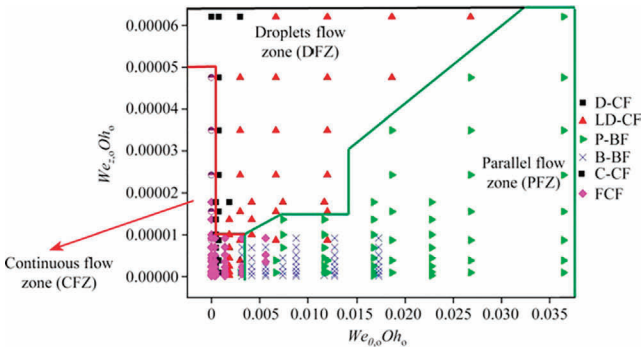

Fig. 12. Universal flow pattern map. Conditions: system = P507–water emulsion; H = 9–19 cm; d_1 = 0.15–0.55 mm; R = 0–700 r·min^{-1}; $Q_{em,in}$=1–8 ml·min^{-1}; T_{in} = 25 °C; T = room temperature (~25 °C).

of tangent direction and vertical direction, The flow patterns of all operation parameters in Fig. 11 are summarized as the universal flow map in Fig. 12 as coordinates.

As shown in Fig. 12, the first type is continuous flow (CFZ), which includes C-CF and FCF, mainly located in the region where $We_{\theta,o} \cdot Oh_o$ and $We_{z,o} \cdot Oh_o$ are both lower. Fig. 13 shows the comparison of E_{total} and E_{up} of different flow patterns. C-CF and FCF have smaller external disturbance in tangential direction and vertical direction, and lower E_{total} and E_{up}. The second type is droplets flow zone (DFZ), which includes D-CF and LD-CF, mainly located in the areas of higher $We_{\theta,o} \cdot Oh_o$ and $We_{z,o} \cdot Oh_o$. D-CF and LD-CF have good E_{total} and E_{up} effects due to certain centrifugal inertia force in tangent direction. The third type is parallel flow zone (PFZ), which includes P-BF and B-BF, mainly in the region where $We_{\theta,o} \cdot Oh_o$ and $We_{z,o} \cdot Oh_o$ are higher. Combined with Fig. 13, although P-BF has the highest E_{total} due to high centrifugal inertia force, RM has a strong internal restriction effect, resulting in a poor E_{up} of P-BF. However, B-BF flow pattern is affected by higher centrifugal inertia force, but the IRM has weak internal limiting effect. Therefore, the E_{up} of the B-BF flow pattern is significantly improved with the retention of excellent E_{total}.

In summary, the universal flow pattern map established in this section can better predict the liquid–liquid two-phase flow pattern of the organic phase and the remaining emulsion. By comparison, the highest demulsification and recovery of organic phase of the IRM (E_{total}) can be achieved when the control is P-BF. However, when B-BF and LD-CF are controlled, the IRM can retain good E_{total} and the E_{up} is significantly improved.

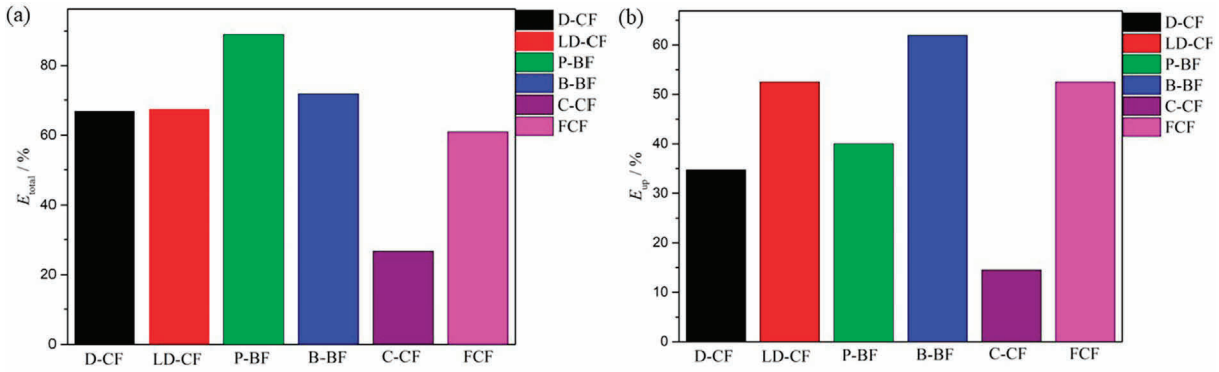

Fig. 13. Comparison of the total demulsification efficiency (E_{total}) and on the demulsification efficiency of the upper outlet (E_{up}) of different flow patterns: (a) E_{total}; (b) E_{up}.

4. Conclusions

Demulsification in a novel IRM was further studied in this paper. This paper mainly draws the following conclusions:

(1) Appropriately increasing the microchannel diameter (d_1) of the IRM makes the IRM maintain a good E_{total} on the one hand, and on the other hand, the ability to separate the organic phase (E_{up}) from the upper outlet can also be significantly improved.
(2) The flow patterns of different equipment structures and operating parameters were drawn. The relation map of the total demulsification efficiency (E_{total}) and universal flow map were further established to provide a certain basis for reasonable and accurate control of the IRM device.

Data Availability

Data will be made available on request.

Declaration of Competing Interest

The authors declare that they have no known competing financial interests or personal relationships that could have appeared to influence the work reported in this paper.

Supplementary Material

Supplementary data to this article can be found online at https://doi.org/10.1016/j.cjche.2022.05.002.

Nomenclature

D	droplet diameter of emulsion, m
d_1	microchannel device geometric diameter, m
E	demulsification efficiency, %
H	height of fluid region, m
$Q_{em,in}$	volumetric flow rates of the emulsion in the inlet, $m^3 \cdot s^{-1}$
R	rotational inner cylinder speed, $r \cdot min^{-1}$
R_1	radius of inner cylinder, m
R_2	radius of outer wall, m
r	organic phase synthesis velocity, m
u_a	aqueous phase synthesis velocity, $m \cdot s^{-1}$
u_o	organic phase synthesis velocity, $m \cdot s^{-1}$
u_z	velocity of aqueous phase in vertical direction, $m \cdot s^{-1}$
u_θ	tangential velocity of aqueous phase, $m \cdot s^{-1}$
$\bar{u}_\theta$	mean tangential velocity of aqueous phase, $m \cdot s^{-1}$
V	volume, ml
μ_o	organic phase viscosity, Pa·s
μ_a	aqueous phase viscosity, Pa·s
φ_o	organic phase content of the initial emulsion
σ	interfacial tension, $N \cdot m^{-1}$

Subscripts

a	aqueous phase
o	organic phase
em	emulsion
up	the upper outlet
low	the lower outlet
remain	the remaining emulsion that has not been demulsified

References

[1] D.S. Ma, H. Yi, C. Lai, X.G. Liu, X.Q. Huo, Z.W. An, L. Li, Y.K. Fu, B.S. Li, M.M. Zhang, L. Qin, S.Y. Liu, L. Yang, Critical review of advanced oxidation processes in organic wastewater treatment, *Chemosphere* 275 (2021) 130104.
[2] J.J. Rueda-Marquez, I. Levchuk, P. Fernández Ibañez, M. Sillanpää, A critical review on application of photocatalysis for toxicity reduction of real wastewaters, *J. Clean. Prod.* 258 (2020) 120694.
[3] Y.Q. Yang, J.X. Guo, Z.F. Cheng, W.M. Wu, J.J. Zhang, J.W. Zhang, Z.G. Yang, D.S. Zhang, New composite viscosity reducer with both asphaltene dispersion and emulsifying capability for heavy and ultraheavy crude oils, *Energy Fuels* 31 (2) (2017) 1159–1173.
[4] P. Kundu, V. Paul, V. Kumar, I.M. Mishra, Formulation development, modeling and optimization of emulsification process using evolving RSM coupled hybrid ANN-GA framework, *Chem. Eng. Res. Des.* 104 (2015) 773–790.
[5] K. Wang, G.S. Luo, Microflow extraction: A review of recent development, *Chem. Eng. Sci.* 169 (2017) 18–33.
[6] P.L. Mills, D.J. Quiram, J.F. Ryley, Microreactor technology and process miniaturization for catalytic reactions—A perspective on recent developments and emerging technologies, *Chem. Eng. Sci.* 62 (24) (2007) 6992–7010.
[7] J. Tan, J.H. Xu, S.W. Li, G.S. Luo, Drop dispenser in a cross-junction microfluidic device: Scaling and mechanism of break-up, *Chem. Eng. J.* 136 (2–3) (2008) 306–311.
[8] G.F. Christopher, S.L. Anna, Microfluidic methods for generating continuous droplet streams, *J. Phys. D: Appl. Phys.* 40 (19) (2007) R319–R336.
[9] F.Y. Ushikubo, F.S. Birribilli, D.R.B. Oliveira, R.L. Cunha, Y- and T-junction microfluidic devices: Effect of fluids and interface properties and operating conditions, *Microfluid. Nanofluidics* 17 (4) (2014) 711–720.
[10] T. Roques-Carmes, H. Monnier, J.F. Portha, P. Marchal, L. Falk, Influence of the plate-type continuous micro-separator dimensions on the efficiency of demulsification of oil-in-water emulsion, *Chem. Eng. Res. Des.* 92 (11) (2014) 2758–2769.
[11] Z.D. Ma, Y.D. Pu, D. Hamiti, M.X. Wei, X. Chen, Elaboration of the demulsification process of W/O emulsion with three-dimensional electric spiral plate-type microchannel, *Micromachines* 10 (11) (2019) 751.
[12] E. Kolehmainen, I. Turunen, Micro-scale liquid–liquid separation in a plate-type coalescer, *Chem. Eng. Process. Process. Intensif.* 46 (9) (2007) 834–839.
[13] D. Ciceri, J.M. Perera, G.W. Stevens, The use of microfluidic devices in solvent extraction, *J. Chem. Technol. Biotechnol.* 89 (6) (2014) 771–786.
[14] C.X. Fan, R. Ma, Y.B. Wang, J.H. Luo, Demulsification of oil-in-water emulsions in a novel rotating microchannel, *Ind. Eng. Chem. Res.* 59 (17) (2020) 8335–8345.
[15] H. Wang, B.X. Quan, X.Q. An, Y. Yang, C. Tian, Advanced decomposition of coking wastewater in relation to total organic carbon using an electrochemical system, *Pol. J. Environ. Stud.* 26 (2) (2017) 941–947.
[16] B. Chakrabarty, A.K. Ghoshal, M.K. Purkait, Cross-flow ultrafiltration of stable oil-in-water emulsion using polysulfone membranes, *Chem. Eng. J.* 165 (2) (2010) 447–456.

[17] M. Hlavacek, Break-up of oil-in-water emulsions induced by permeation through a microfiltration membrane, *J. Membr. Sci.* 102 (1995) 1–7.
[18] S. Kasemset, A. Lee, D.J. Miller, B.D. Freeman, M.M. Sharma, Effect of polydopamine deposition conditions on fouling resistance, physical properties, and permeation properties of reverse osmosis membranes in oil/water separation, *J. Membr. Sci.* 425–426 (2013) 208–216.
[19] G.L. Mo, H. Liu, S. Dai, Y.B. Wang, J. Li, J.H. Luo, Extraction of Fe^{3+} from NaH_2PO_4 solution in a spiral microchannel device, *Chem. Eng. Process. Process. Intensif.* 144 (2019) 107654.
[20] F. Kubota, M. Goto, F. Nakashio, Extraction of rare earth metals with 2-ethylhexyl phosphonic acid mono-2-ethylhexyl ester in the presence of diethylenetriaminepentaacetic acid in aqueous phase, *Solvent Extr. Ion Exch.* 11 (3) (1993) 437–453.
[21] Z. Chen, W.T. Wang, F.N. Sang, J.H. Xu, G.S. Luo, Y.D. Wang, Fast extraction and enrichment of rare earth elements from waste water *via* microfluidic-based hollow droplet, *Sep. Purif. Technol.* 174 (2017) 352–361.
[22] M.A. Rother, R.H. Davis, Simplified model for droplet growth in shear flow, *AIChE J.* 49 (2) (2003) 546–548.
[23] B.E. Priore, L.M. Walker, Coalescence analysis through small-angle light scattering, *AIChE J.* 47 (12) (2001) 2644–2652.
[24] S.P. Lyu, F.S. Bates, C.W. Macosko, Coalescence in polymer blends during shearing, *AIChE J.* 46 (2) (2000) 229–238.
[25] Y.C. Zhao, G.W. Chen, Q. Yuan, Liquid–liquid two-phase flow patterns in a rectangular microchannel, *AIChE J.* 52 (12) (2006) 4052–4060.
[26] F.N. Sang, Z. Chen, Y.D. Wang, J.H. Xu, Dynamic formation and scaling law of hollow droplet with gas/oil/water system in dual-coaxial microfluidic devices, *AIChE J.* 64 (2) (2018) 730–739.
[27] F. Scheiff, M. Mendorf, D. Agar, N. Reis, M. Mackley, The separation of immiscible liquid slugs within plastic microchannels using a metallic hydrophilic sidestream, *Lab Chip* 11 (6) (2011) 1022–1029.
[28] C. Chao, G.W. Xu, X.F. Fan, Effect of surface tension, viscosity, pore geometry and pore contact angle on effective pore throat, *Chem. Eng. Sci.* 197 (2019) 269–279.
[29] A.L. Dessimoz, L. Cavin, A. Renken, L. Kiwi-Minsker, Liquid–liquid two-phase flow patterns and mass transfer characteristics in rectangular glass microreactors, *Chem. Eng. Sci.* 63 (16) (2008) 4035–4044.
[30] M.N. Kashid, A. Renken, L. Kiwi-Minsker, Influence of flow regime on mass transfer in different types of microchannels, *Ind. Eng. Chem. Res.* 50 (11) (2011) 6906–6914.
[31] E. Buckingham, On physically similar systems; Illustrations of the use of dimensional equations, *Phys. Rev.* 4 (4) (1914) 345–376.
[32] S.K.R. Cherlo, S. Kariveti, S. Pushpavanam, Experimental and numerical investigations of two-phase (liquid–liquid) flow behavior in rectangular microchannels, *Ind. Eng. Chem. Res.* 49 (2) (2010) 893–899.
[33] A.V. Minakov, A.A. Shebeleva, A.A. Yagodnitsyna, A.V. Kovalev, A.V. Bilsky, Flow regimes of viscous immiscible liquids in T-type microchannels, *Chem. Eng. Technol.* 42 (5) (2019) 1037–1044.
[34] M. Darekar, K.K. Singh, S. Mukhopadhyay, K.T. Shenoy, Liquid–liquid two-phase flow patterns in Y-junction microchannels, *Ind. Eng. Chem. Res.* 56 (42) (2017) 12215–12226.